Supporting Information (SI) Appendix

A kinetic model of the aggregation of alpha-synuclein provides insights into prion-like spreading

Marija Iljina, Gonzalo A. Garcia, Mathew H. Horrocks, Laura Tosatto, Minee L. Choi, Kristina A. Ganzinger, Andrey Y. Abramov, Sonia Gandhi, Nicholas W. Wood, Nunilo Cremades, Christopher M. Dobson, Tuomas P. J. Knowles and David Klenerman

Correspondence may be addressed to: tpjk2@cam.ac.uk, dk10012@cam.ac.uk

Contents:

1. Supporting Methods

1.1. Analysis of kinetic traces from sm-FRET.

FRET efficiency histograms for the single-molecule FRET (sm-FRET) aggregation experiments at 35, 70 and 140 μM starting protein concentrations showed two distinguishable distributions attributed to low- and high-FRET oligomer types (Fig. 2), and separate kinetic traces for the both types were obtained. The FRET histograms of the two separate size groups were globally fitted (eq. S1, Origin 7.0) to a single Gaussian distribution for 2-5-mers, or a double Gaussian distribution for 6-150-mers, using GaussAmp functions:

$$y = y_0 + A\exp\left(-\frac{(x-x_c)^2}{2w^2}\right)$$
$$y = y_0 + A\exp\left(-\frac{(x-x_c)^2}{2w^2}\right) + A_2\exp\left(-\frac{(x-x_{c2})^2}{2w_2{}^2}\right) \quad \text{(S1)}$$

Table S1. Parameters from the global fitting to GaussAmp functions (eq. S1). Error is one SD from N=6, where N is a dataset from a separate experiment.

conc / μM	Small (2-5-mers)				Large (5-150-mers)							
	x_c	SD(x_c)	w	SD(w)	x_c	SD(x_c)	w	SD(w)	x_{c2}	SD(x_{c2})	w_2	SD(w_2)
35	0.532	0.005	0.087	0.002	0.399	0.066	0.105	0.010	0.641	0.017	0.0921	0.009
70	0.515	0.033	0.236	0.357	0.336	0.007	0.114	0.032	0.654	0.007	0.0951	0.009
140	0.539	0.007	0.085	0.003	0.423	0.038	0.099	0.008	0.629	0.010	0.0859	0.005

where A and A_2 are the amplitudes, x_c and x_{c2} the centres, corresponding to average FRET efficiency values, w and w_2 the widths of the distributions. The centres and the widths were kept constant, and the amplitudes varied. The resulting global fitting parameters are listed in Table S1. The fits using the global parameters accurately described individual histograms up to (and including) 33 hours, the early aggregation time period which was used for modelling. Within this time period, the data from six separate experiments at a chosen concentration could be described by close fitting parameters, with fits using global parameters successfully converging with R^2 values above 0.95 in all cases, and close to zero residual values for individual histograms. The fitted Gaussian distributions were integrated and divided by histogram bin width (0.05) to give the total number of oligomers in each population for each timepoint. Further, the sum of the number of small and low-FRET large oligomers was taken to yield the total number of low-FRET oligomers at 35, 70 and 140 μM. The classification of small oligomers as low-FRET species was consistent with our previous study (1). The total number of high-FRET oligomers was derived from the high-FRET populations at 6-150-mers. Data at 0.5, 5 and 10 μM starting concentrations showed a single broad peak in FRET efficiency histograms at all sizes (Fig. 2 in the Main Text, Fig. S7). These were integrated and divided by histogram bin width (0.05) to give the total number of oligomers for each timepoint.

In this analysis, for 35-140 μM data we observed a 20-70 % reduction in χ^2 upon fitting the individual FRET histograms with double-Gaussian functions in comparison to the single-Gaussian fits, with the highest reduction occurring for the histograms of late timepoints. In the case of 0.5-10 μM data, on average, there was a < 10 % reduction in χ^2 to fits with a double Gaussian function. Since at least a 20 % reduction in χ^2 is considered significant for the introduction of an additional Gaussian function, as has been previously reported (2, 3), double-Gaussian fits were only used for the 35-140 μM data.

The resulting numbers of oligomers, plotted against aggregation time, formed the basis of the oligomer kinetic traces. In order to obtain a more conventional representation of the kinetic traces, showing the change in oligomer concentration with time, further corrections were performed. Firstly, the numbers of oligomers were normalised to the global average monomer bursts, taken over the first 9 hours of aggregation, where the monomer bursts did not undergo a rapid decrease due to monomer depletion. (To note, the value of the average monomer bursts was twice the average value of the bursts from Alexa Fluor 488, AF488-labelled monomer, to account for the 1:1 stoichiometry of the AF488 and the "invisible" AF594 monomer). This gave an approximate estimate of oligomer fraction in the samples. Subsequently, the fraction was multiplied by the starting total protein concentration (μM) to give estimated oligomer concentrations. The kinetic traces of monomer depletion were obtained from the selected monomeric burst counts above the threshold, normalised to the monomeric burst counts at time zero to give the monomer fraction, and multiplied by the starting bulk protein concentration.

We note that the used method for selecting monomeric and oligomeric events from raw experimental data is threshold-dependent. Nevertheless, the resulting estimated oligomer concentration at 70 μM is in agreement with the values obtained in the previously reported sm-FRET measurements, utilising similar instrumentation with static sample detection (1), and more recent results utilising fast flow (4), as well as the previous bulk quantitative SEC calibration (1); and the used method for the measurement of monomer concentration has been validated in our recent study by quantitative SDS-Page (5).

1.2. Bulk THT measurement.

Bulk THT assays were performed to monitor fibril formation at our incubation conditions. For the assays, unlabelled wild-type (wt) alpha-synuclein (αS) was used, and the same buffer and incubation conditions as for the labelled samples. The aliquots were withdrawn at the same time intervals as for the sm-FRET measurements. Withdrawn aliquots were pre-mixed with thioflavin-T (THT) solution to contain 18 μM of this dye. Measurements were performed on Cary Eclipse spectrometer with 440 nm excitation and emission at 470-600 nm. Maximum intensity values from the background-corrected fluorescence spectra were plotted against incubation time (Fig. S1).

1.3. TEM Imaging.

For the TEM imaging, the sample preparation was the same as for the sm-FRET experiments, and labelled αS was used. 10-15 µL volumes of the samples were applied onto carbon-coated 400-mesh copper grids (EM Resolutions) for 5 minutes, and washed with distilled water. Negative staining was carried out by using 2 % (w/v) uranyl acetate. TEM images were acquired using Tecnai G2 microscope (13218, EDAX, AMETEK) operating at an excitation voltage of 200 kV.

1.4. Apparent oligomer size distributions from sm-FRET experiments.

In the sm-FRET experiments, the apparent size distributions of oligomers were derived using the fluorescence intensity values of the simultaneous bursts, according to the following equation:

$$Apparent\ \ size = 2 \times \left(\frac{I_D + \gamma^{-1} I_A}{I_{Dmonomer}} \right) \tag{S2}$$

where I_D is the donor intensity in the presence of an acceptor, I_A is the acceptor intensity and γ is the gamma factor specific to the instrument (0.99), which accounts for the relative detection efficiencies of the dyes and their quantum yield, and $I_{Dmonomer}$ is the average intensity of donor monomers. The expression estimates the number of donor monomers per oligomer, and the factor of 2 is due to assumed 1:1 dye stoichiometry in the oligomers, the assumption valid for the ensemble average analysis. Large species, either occupying neighbouring bins, or more than 150-mers in size, were excluded, as these were assumed to originate from fibrils. These size distributions are termed "apparent" as they serve to broadly reflect the changes in the average populations of oligomer sizes. The determination of exact physical sizes of individual oligomers of αs is beyond the scope of this method.

During the aggregation process, we observed an increase in apparent oligomer sizes, which occurred together with the overall increase in numbers of oligomers (Fig. S8). This growth was present only during the early reaction times, and subsequently the size distributions did not undergo significant changes upon prolonged incubations. During the first two days, oligomers with similar apparent size distributions were formed at all starting protein concentrations.

1.5. Apparent oligomer size distributions from TIRFM measurements.

To confirm the similarity in the fluorescence-derived apparent size distributions of αS oligomers formed at the various protein concentrations, we performed Total Internal Reflection Fluorescence Microscopy (TIRFM) measurements in addition to the confocal experiments using αS samples with 5 μM and 70 μM starting concentrations. Solution-based sm-FRET technique used in this work employs flow and a focused Gaussian laser beam to excite the confocal volume. The protein aggregates can still take different paths through the excitation region potentially broadening the detected intensities and affecting the derived apparent size distributions, and may mask any possibly present differences. In order to eliminate the effect of this inhomogeneous excitation on the resulting apparent size populations, we used immobile oligomers and the wide-field imaging method, TIRFM, to derive the apparent size distributions from fluorescence intensities in an analogous way to the estimation used in the confocal measurement, as detailed below (eq. S3, S4). The results are shown in Figure S9, and the apparent size distributions of oligomers are similar at 5 μM and 70 μM.

TIRFM sample preparation

For TIRFM imaging, αS was 1:1 AF488 and AF647 dual-labelled, and buffer and incubation conditions were the same as for the sm-FRET confocal experiments. Samples with starting protein concentrations of 5 and 70 μM were incubated for > 54 hours to allow characterisation of oligomers at the steady state. Borosilicate glass slides (631-0122, VWR International, 20x20 mm) were cleaned by argon plasma (PDC-002, Harrick Plasma cleaner) for 1.5 hours. Subsequently, frame-seal slide chambers (SLF-0601, Bio-rad, Hercules, CA, USA, 9x9 mm) were attached to the glass and 70 μL Poly-L-lysine (P4707-50ML, Sigma-Aldrich, mol wt 70,000-150,000) added on top and incubated for 30 minutes before being washed with Tris buffer of the same composition as used for the aggregations. Prior to adding protein samples, each glass slide batch was checked for the absence of fluorescent artefacts by imaging a buffer-containing blank slide. For imaging, protein was diluted to 100 pM concentration, added to the coverslide and incubated for 10 minutes allowing oligomers to adhere to the surface.

TIRFM data acquisition

Imaging was performed using a home-built TIRFM setup, described before (6). Inverted Nikon Eclipse TE200 microscope (Nikon Corporation, Tokyo, Japan) was used and a 60× magnification (Plan Apo TIRF, NA=1.45) oil-immersion objective (Nikon Corporation). Dual illumination by a diode laser operating at 488 nm (PC13589; Spectra Physics, Canada) and a He:Ne laser at 633 nm (25LHP, Melles

Griot, CA) were utilized. The TIRF mode was achieved by adjusting the position of aligned laser beams before they enter the objective. Fluorescence signal was split by a DualView (Optical Insights, Lilburn, CA) mounted dichroic and after being separated into two colours was simultaneously recorded on each half of the chip of Photometrics Cascade II:512 EMCCD camera (Photometrics, Tucson, AZ). To adjust the overlap of images in both channels, a grid with evenly-separated holes in gold-on-glass was used. Data were acquired using MicroManager (7), and the dimensions of the recorded images were 512×512 pixels, with a pixel size of 107×107 nm in the sample plane. The acquired datasets consisted of short video files, recorded by stream acquisition of 50 images with an exposure time of 100 ms. A new cover slide was used for every 25 videos to avoid recording pre-bleached species. 200 videos were recorded per protein sample, and three separate aggregated samples were measured for 5 μM concentration (total of 600 videos), and the same number for 70 μM concentration. All measurements were made at ambient temperature (c.a. 21 ^{o}C).

TIRFM data analysis

Using TIRFM data, apparent sizes of oligomers were determined by normalising oligomer fluorescence intensities to the average monomer brightness as in our previous work (8). Briefly, the data were analysed using custom-written MATLAB software (R2011b, MathWorks, Natick, MA). The fluorescence images were background-corrected and spots detected above empirically determined thresholds, (5 and 7 SD above the background for the blue and the red channel) chosen to be in agreement with what is detected by eye.

Firstly, by analysing predominantly monomeric data the average 647-labelled monomer intensity ($I_{monomer}$) was found. It was defined as the average intensity of detected spots in the first frame prior to bleaching (N=5123) minus the average intensity of the spots in the last frame after the bleaching and was 41 ± 0.6 (SEM) counts.

Subsequently, oligomer intensities were extracted from the red (Alexa Fluor 647 fluorescence) channel (I_{red}). Oligomers were distinguished from monomers by detecting coincident spots in the red and the blue channels, with a requirement for the colocalized particles to stay within 300 nm of each other to account for any limitations in image registration (c.a. 120 nm) and localisation precision (c.a. 50 nm for both detection in the blue and red channels). A centroid fit to the bright objects was followed by a Gaussian fit, and the extracted intensity values corresponded to the amplitudes of the Gaussian fits (9). The intensities were averaged over multiple frames prior to photobleaching.

To determine the apparent sizes, the oligomer intensities were doubled to account for the "invisible" blue fluorophores (since oligomers were created by aggregation of a 1:1 mixture of Alexa Fluor 488 and Alexa Fluor 647 labelled protein monomers), and divided by average monomer brightness determined:

$$Apparent\ size = \frac{2 \times I_{red}}{I_{monomer}} \tag{S3}$$

The apparent size values were represented as histograms with bin-widths of 1, with combined data from three separate samples per starting concentration (from 600 videos per concentration). The size distributions were corrected to account for potentially present non-coincident singly-labelled oligomers, by multiplying each size population by the factor:

$$F_{one-colour} = \frac{2^x}{2^x - 2} \quad where\ x\ is - mer \geq 2 \tag{S4}$$

1.6. TIRFM on-the-slide seeding experiments.

The experiments were performed using AF647-labelled αS at 70 µM after 29 hours of incubation at the same conditions as for the sm-FRET experiments, and AF647-labelled αS monomeric samples. Borosilicate glass slides (631-0122, VWR International, 20x20 mm) were plasma-cleaned and coated with Poly-L-lysine (P4707-50ML, Sigma-Aldrich, mol wt 70,000-150,000). Prior to imaging the protein samples, the glass slides were checked for the absence of fluorescent artefacts by imaging a buffer-containing blank slide. Subsequently, a 70 µM sample after 29 hours was pre-mixed with THT dye (Sigma-Aldrich) and applied on the slide at ~ 2 µM concentration of αS and 5 µM concentration of THT (Sigma-Aldrich), in order to image immobilised THT-active aggregates. The imaging was performed using a home-built TIRFM setup, using a 405 nm excitation laser (Oxxius, LBX-LD) operated at the power of approximately 8 mW, measured at the back-port of the Olympus IX-73 microscope, equipped with a 60x objective (N.A.=1.49, ApoN 60XOTIRF, Olympus). The emission signal was imaged onto the EMCCD camera (Photometrics, Evolve Delta 512). The control of the hardware was performed using custom-written MicroManager software (US National Institute of Health) (7). All measurements were made at ambient temperature (c.a. 21 °C). After immobilising the aggregates on the surface of the coverslide, αS-AF647 monomer, pre-mixed with THT, was added dropwise in excess, and the coverslide was imaged, referred to as "t0 image". To note, because the samples are stained by THT, the added monomer remains invisible, and only beta-sheet-containing aggregates can be detected. The acquired data consisted of short video files, recorded by stream

acquisition of 100 images with an exposure time of 50 ms, and images were created by taking the average of the corresponding 100 image stacks using Image J (NIH) software. The coverslide was subsequently incubated stationary, and the same field of view as at t0 was re-imaged over time. The images taken at later times were overlapped with the t0 image (Image J), and the largest changes in the morphology of the initially present THT-active aggregates occurred after 10-18 hours, after which time the aggregates were observed to elongate. The procedure was repeated at least three times and all results agreed. Representative overlapped images at t0 and t18, after 18 hours of incubation, are shown in Figure S11.

1.7. Critical aggregation concentration measurement.

Fibrils were prepared by incubating 70 µM AF-488 labelled αS for 7 days under the same conditions as for the sm-FRET experiments. Subsequently, pellets were collected by centrifugation at 12,800 x g for 15 minutes, washed with fresh buffer and centrifuged for 5 minutes. The washing step was repeated twice. Following this, the pellets were re-suspended in fresh Tris buffer (100 µL) ensuring the excess of fibrillar material. The resulting samples were incubated under static conditions at 37^{o}C for 3 days, and centrifuged for 15 minutes at 12,800 x g prior to measurements. To confirm the attainment of the steady state, identical samples were incubated for longer (7 days).

Data were acquired using the same single-molecule setup as for the sm-FRET measurements, operating in the 488/647 excitation mode. The concentration of αS in the supernatant, which included monomeric and oligomeric species released from the fibrils, was estimated by relating the burst counts of the measured soluble supernatants to the burst counts from a 488/647 dual-labelled DNA standard (Atdbio) of precisely known concentration. 488 nm laser illumination was used for the measurement of supernatants, and for the generation of the calibration curve in the 488 channel. The measurements were stationary, with solutions placed on a glass coverslide and focussing the laser beam 10 µm into the solution, followed by acquisition for 200 s, with 1 ms time-bins (chosen according to the expected residence time in the confocal volume at these conditions), 8000 bins per frame and a total of 25 frames. Initially, a calibration curve was recorded using a dual-labelled 40 base pair DNA duplex, generated by annealing a 1/1 mixture of double-HPLC purified complementary synthetic oligonucleotides (Atdbio) with the following sequence:

AlexaFluor488-TAGTGTAACTTAAGCCTAGGATAAGAGCCAGTAATCGGTA

AlexaFluor647-TACCGATTACTGGCTCTTATCCTAGGCTTAAGTTACACTA

Calibration was made with the reference to a triplicated measurement of the standard at a range of concentrations, which resulted in a linear increase in the number of bursts in the 488 channel above

an arbitrarily chosen fixed threshold (10 counts bin^{-1}) with the sample detection concentration (0-250 pM).

Subsequently, the supernatants collected from the fibrillar samples were diluted in Tris buffer (serial dilution) by a factor of $1x10^5$ and recorded as described. The number of bursts above the same threshold as for the standard (10 counts bin^{-1}) was counted and converted to the detection concentration, and subsequently to the bulk concentration using the dilution factor. The results are summarised in Table S2. Comparable numbers of bursts were obtained in the samples after 3 and 7 days of incubation.

Table S2: Measurement of the total soluble species (monomers + oligomers) above fibrillar pellets. Calibration to AF488 and 647 dual-labelled 40 base pair DNA strand, by the reference to the bursts in the 488-channel. Error is one SD from N=6, where N is a fibrillar sample.

Average number of bursts (N=6)	SD	[SM] / pM	SD ([SM]) / pM	[Bulk] / nM	SD ([Bulk]) / nM
1349	351	7.3	1.8	730	200

1.8. ROS measurements.

We have previously reported that oligomers can be taken up rapidly by neurons and astrocytes and that the high-FRET oligomers promote the production of reactive oxygen species (ROS) when applied to primary neuronal cultures (1). In this study, we firstly compared the effect on the neuronal cells of addition of oligomers prepared at 70 µM versus oligomers prepared at 5 µM, when the aggregation was stopped at the same time for both concentrations (Fig. S15 A and B). Secondly, we determined how low a concentration of oligomers could be added that still resulted in detectable ROS.

Firstly, dose-response experiments were performed using either AF647 or unlabelled wt 70 µM and 5 µM αS samples after 29 hours of incubation at the same conditions as for the sm-FRET experiments. The imaging was performed by two methods, using either a confocal miroscope or a CCD camera, with qualitatively agreeable results. Using the confocal microscope, the rate of oxidation of cytosolic hydroethidium was measured as the intensity of the fluorescence emitted at 580 nm at basal levels and then on application of oligomers from either the 5 or 70 µM samples. Parallel experiments using CCD measured the rate of increase in the ratio of cytosolic Het fluorescence between the oxidised and non-oxidised form at basal levels for 3 minutes, and then on exposure to oligomers from either the 5 or 70 µM samples. Overall, data were generated from four coverslips for every applied oligomer concentration, in two different cell and protein preparations. The rate of increase in fluorescence (of either the oxidised Het on confocal, or the ratio of oxidised:non-oxidised on CCD) was normalised to 100 % for the basal level of ROS production prior

to application of oligomers. A representative experiment from the confocal based assay is shown in Fig. S15. In both cases the oligomers were found to induce ROS, confirming that the oligomers produced at both 70 and 5 μM are damaging to neuronal cells.

Secondly, using the unlabelled αS, we gradually diluted the oligomers produced at 70 μM to low concentrations, and the lowest oligomer concentration to clearly produce ROS was 50 pM, beyond which we observed a much more variable response from cells. At 50 pM, the observed increase was 244 ± 9 % (SEM, N(cells)=156-164 per experiment), relative to the basal level of 100 %, during a 10 minute detection. 50 pM concentration corresponds to 30 oligomers in a cell-like volume $(10\ \mu m)^3$. To note, although it is known from the previous ROS studies that the concentration of fibrils needs to be higher in order to produce comparable ROS levels (10), the determination of the exact threshold concentration of fibrils required was beyond the scope of these experiments.

ROS experimental procedures

The protein samples of AF647 labelled A90C (the emission from AF647 did not interfere with Het signal), or of unlabelled wt αS, were incubated under the same aggregation conditions as for the kinetic measurements, with the starting protein concentrations of 5 and 70 μM. The aggregated samples were withdrawn after 29 hours of incubation prior to measurements. For the measurements, cells were washed with HBSS containing Ca^{2+} and Mg^{2+} (Gibco, UK) once and briefly incubated with 1.25 μM dihydroethidium (Het, Invitrogen, UK) for 2-3 minutes prior to live-cell imaging. Het was present during the experiment. Confocal images were obtained using a Zeiss 710 LSM with an integrated META detection system. Oxidized Het fluorescence was measured by excitation with the 543 nm laser line and a 560 nm long pass filter (×40 objective). Illumination intensity was kept to a minimum to avoid phototoxicity. Addition of a bright field image allowed separation between neurons and glia that are visibly different and are situated on different focal planes. Data were acquired and analyzed using ZEN2009 software.

The production of ROS was also measured on an epifluorescence inverted microscope equipped with a ×20 fluorite objective. In these experiments, the ratio of the oxidized to reduced forms of the Het dye was measured. Excitation at 540 nm and emission recorded above 560 nm were used to quantify the oxidized form (ethidium), whereas excitation at 360 nm and emission collected from 405 to 470 was used for the reduced form (hydroethidium). Phototoxicity and photobleaching of cells were minimized by limiting the light exposure to the time of acquisition of the images. Fluorescent images were acquired with a frame interval of 10 seconds. Data were analyzed using software from Andor IQ (Belfast, UK).

2. Supporting Figures

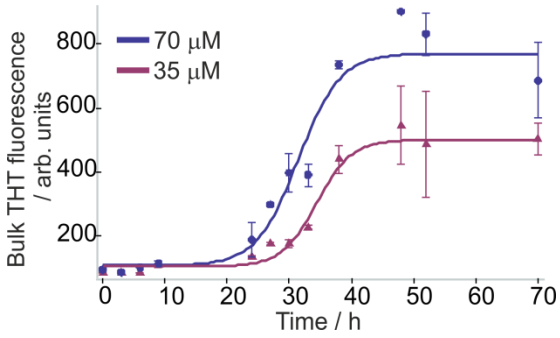

Fig. S1. Bulk THT fluorescence time traces, showing the progression of fibril formation for unlabelled wild-type αS at the same incubation conditions as for the sm-FRET experiments. (SD, N=3). Fit to sigmoid function with $t_{1/2}$(70 µM)=31.5±1.3 hours and $t_{1/2}$(35 µM)=34.3±0.9 hours (error from the fit.) Early oligomeric species**,** particularly ones present during the first day of aggregation, cannot be studied by this method, justifying the use of sm techniques in this study.

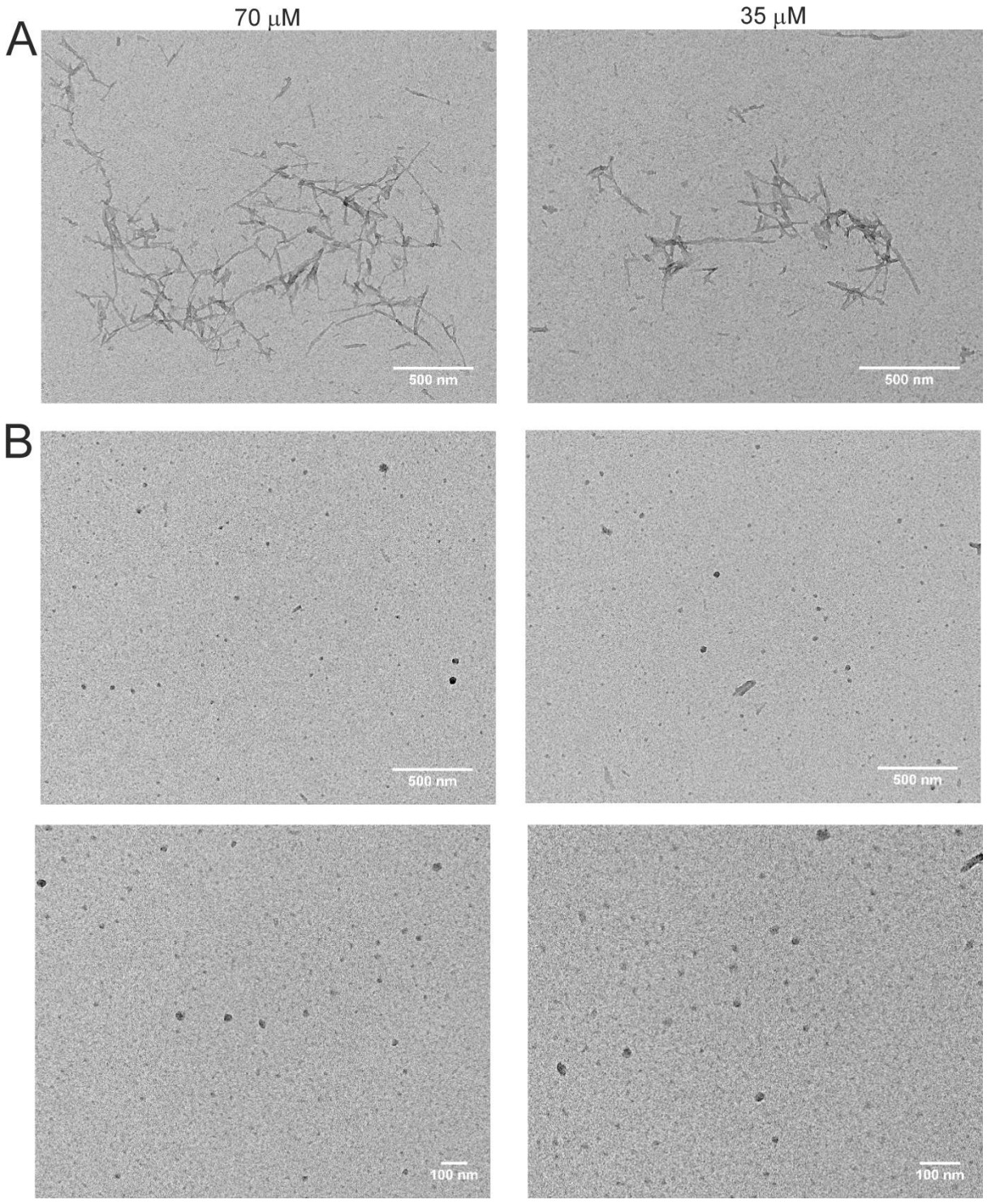

Fig. S2. TEM images of dual-labelled αS samples with the starting protein concentrations of 70 μM and 35 μM, incubated for 24 hours at the same conditions as for the bulk THT experiments and sm-FRET measurements. (A) Samples without spindown at 24 hours contain a mixture of long fibrils and small spherical oligomers. (B) Supernatants of the same samples following centrifugation for 10 minutes at 12,800 x g. Spherical oligomers and a low number of short protofibrils are present in the supernatant, and are therefore separated from the large fibrils.

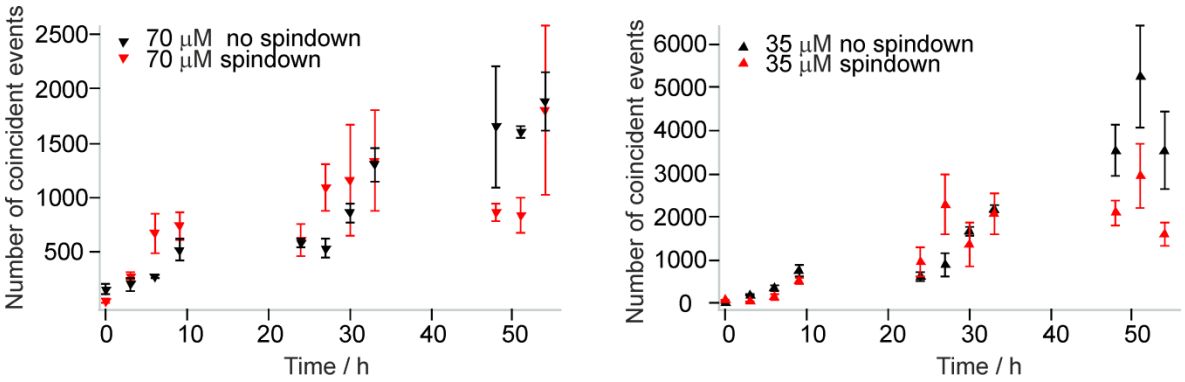

Fig. S3. Control sm-FRET measurements to assess a potential contribution from large fibrils to the signal in the oligomer kinetic profiles (SEM, N=3). Dual-labelled samples of αS are incubated at 70 µM and 35 µM starting concentrations, and the sm-FRET measurements are carried out on the samples either directly withdrawn from the incubating solutions (shown in back), or on the supernatants of the samples after centrifugation for 10 minutes at 12,800 x g (shown in red). The results are represented in numbers of coincident events versus incubation time. The data are broadly unaffected within the first 33 hours, the time period used for the subsequent fitting. Comparable numbers of aggregates present at this time regardless of the presence or the absence of centrifugation confirm that the signal present at this time mainly arises from the small oligomeric species, and that fibrils present at 24-33 hours do not contribute to the measurement. At later times, which are not used in the modelling, higher numbers of aggregates are detected in the samples without centrifugation, presumably due to a contribution from fibrils which are highly abundant at this late incubation time. All of the subsequent sm-FRET measurements are performed without centrifugation, unless otherwise stated.

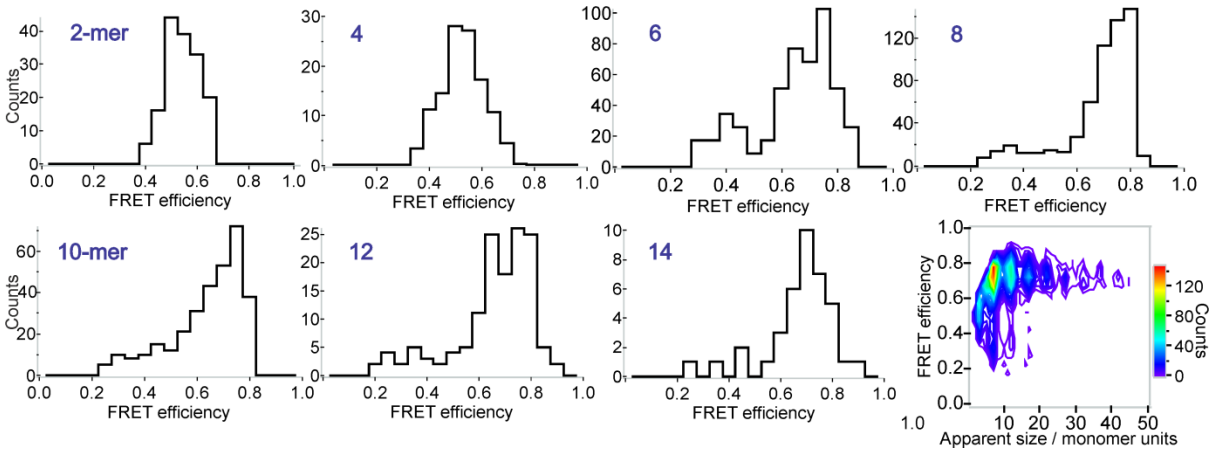

Fig. S4. Appearance of FRET efficiency histograms resulting from a 35 µM sample of αS after 30 hours of incubation and extended detection time (2500 s), split into individual apparent sizes. Typically, the histograms display a single peak below 5 monomer units, due to the applied thresholds and low photon counts from these small species, and start to show two FRET populations at 6 monomer units and higher. This is the basis for splitting the sm-FRET data into size groups of 2-5-mers and 6-150-mers.

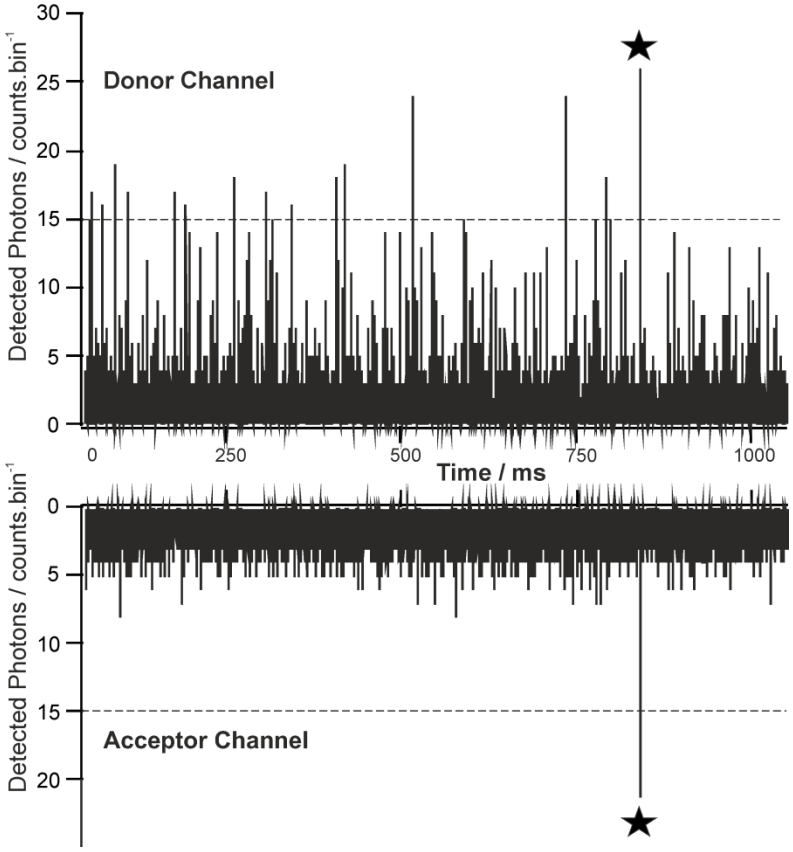

Fig. S5. Photon traces resulting from 1 s of raw experimental data from the sm-FRET measurement, using 488 nm laser excitation and detection in both the donor and the acceptor channels. Photon traces of 400 s duration were recorded for the analysis of every individual timepoint, unless otherwise stated. Thresholds of 15 counts per bin, chosen according to the MaxQ approach (11), were applied to select either the simultaneous events in the donor and the acceptor channel, arising from oligomers (marked with black star), or to count individual monomeric bursts above the threshold in the donor channel. The chosen concentration for the measurement allowed discrete monomeric bursts above the applied threshold, and multiple occupancy events were negligible as verified using the desynchronisation approach (2).

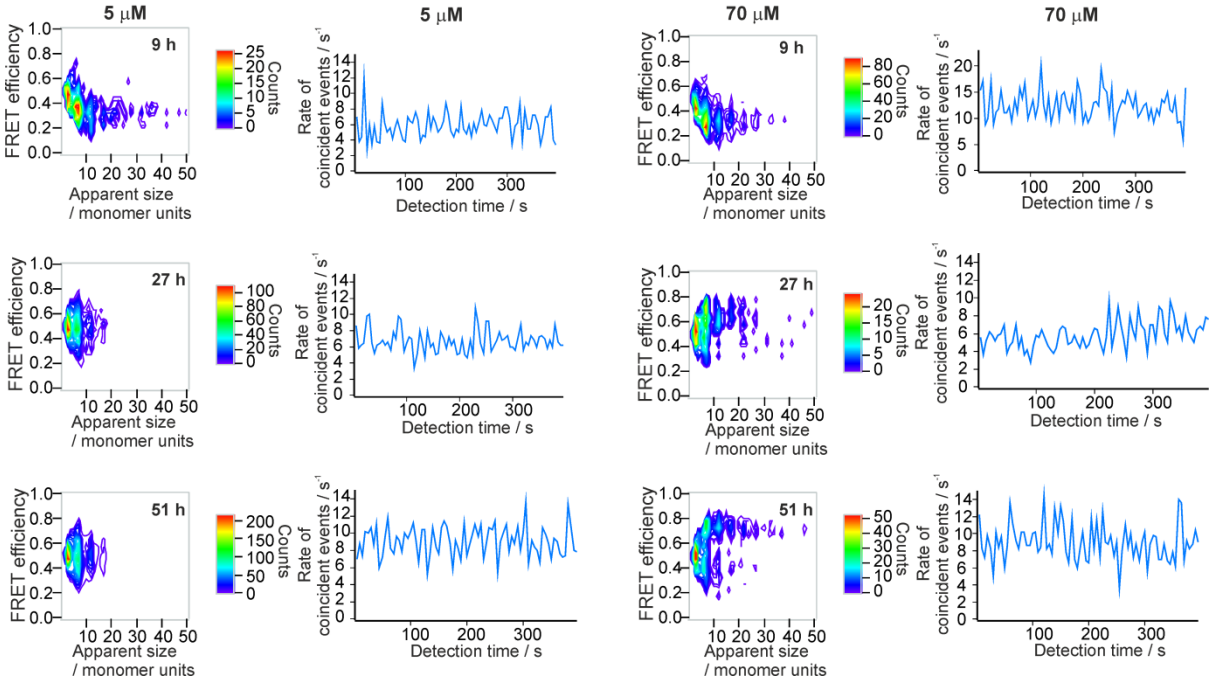

Fig. S6. Evidence for oligomer stability during sm-FRET detection. The plots of rate of coincident events against time, resulting from 400 s measurement time, and the corresponding contour plots of FRET efficiency against apparent oligomer sizes for 70 and 5 μM samples after 9, 27 and 51 hours of aggregation, containing varying proportions of low-FRET and high-FRET sub-populations. Stable rate of coincident events in these experiments suggests the absence of gradual oligomer dissociation during the measurements.

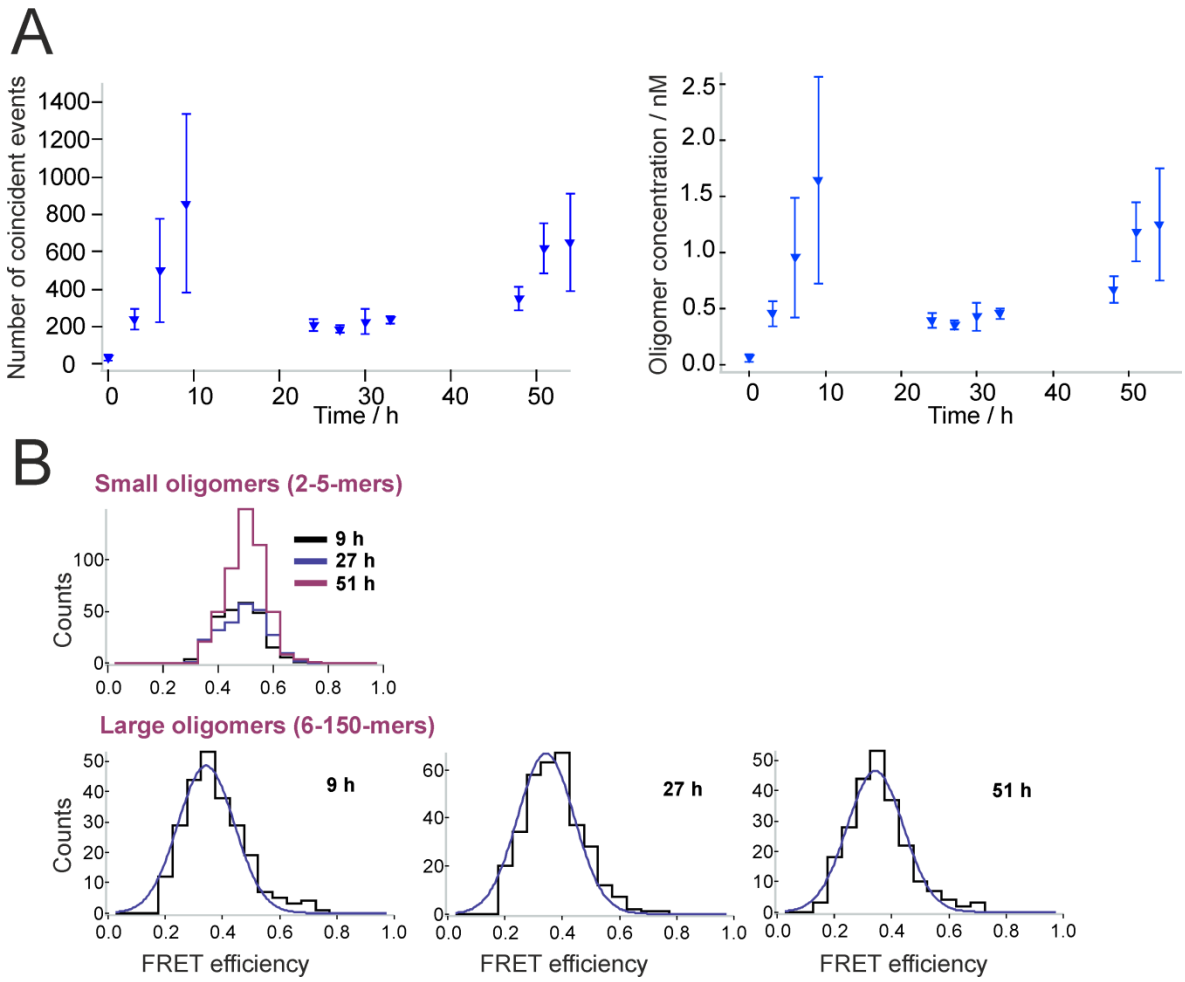

Fig. S7. Sm-FRET results of αS aggregation at 0.5 μM starting protein concentration. (A) Oligomer kinetic profiles, displayed both in numbers of oligomers versus incubation time, and the concentrations of oligomers versus incubation time (SEM, N=6). (B) Appearance of FRET efficiency histograms of samples with 0.5 μM starting protein concentrations. The histograms of large oligomers are fitted to the single-Gaussian function, with E(global)=0.34. No shift in the centres of the histograms is observed within the time of the aggregation experiment.

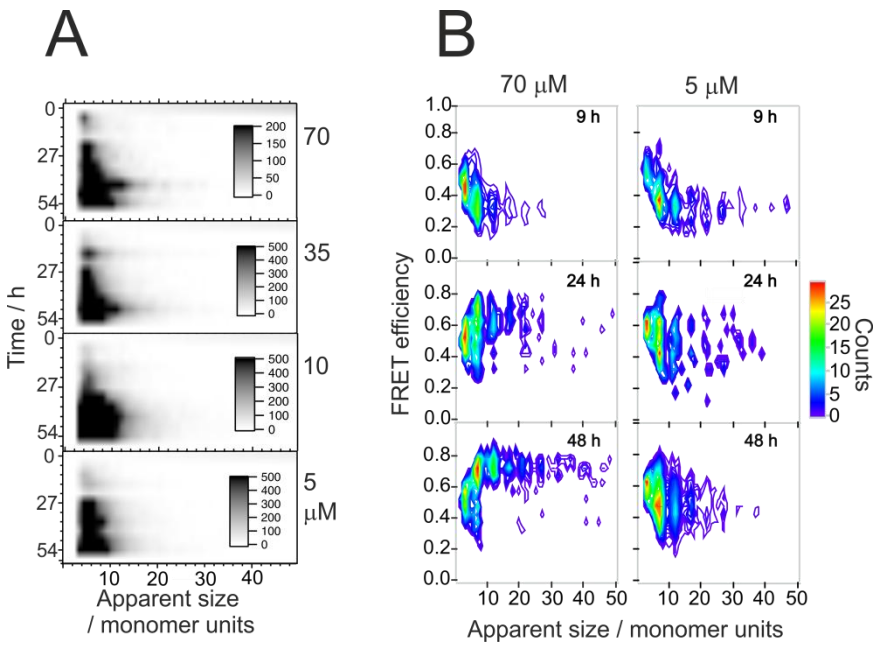

Fig. S8. (A) Number density histograms showing the evolution of apparent oligomer size distributions due to αS oligomer growth in the aggregation experiments for 5 – 70 μM samples. (B) Representative contour plots of FRET efficiency against populated apparent oligomer sizes of 70 and 5 μM samples after 9, 24 and 48 hours of aggregation. The conversion process from low-FRET oligomers to high-FRET oligomers at 70 μM is observed.

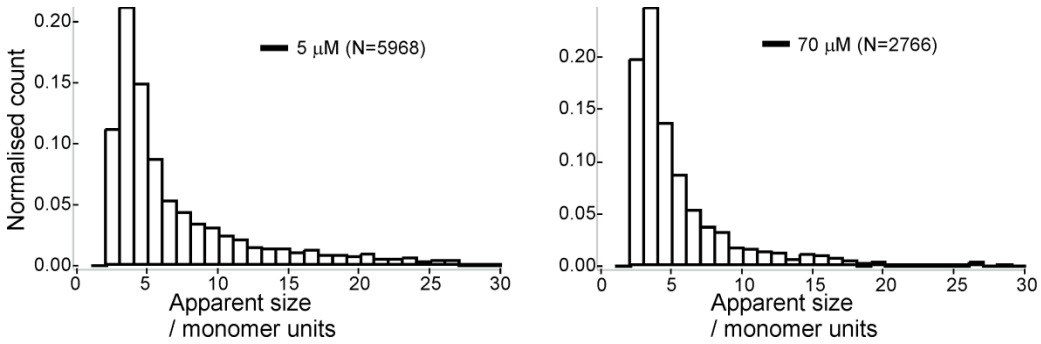

Fig. S9. Apparent size distributions, derived from TIRFM measurements of oligomers in 5 and 70 μM samples at the steady state. Similarly to the apparent size estimation from the sm-FRET measurements, the values are derived from fluorescence intensities, as detailed in the Supporting Methods section 1.5. The results are in close agreement with the data from the sm-FRET measurements. Histograms are normalized to the total area. There is no difference in the distributions derived from 5 and 70 μM samples.

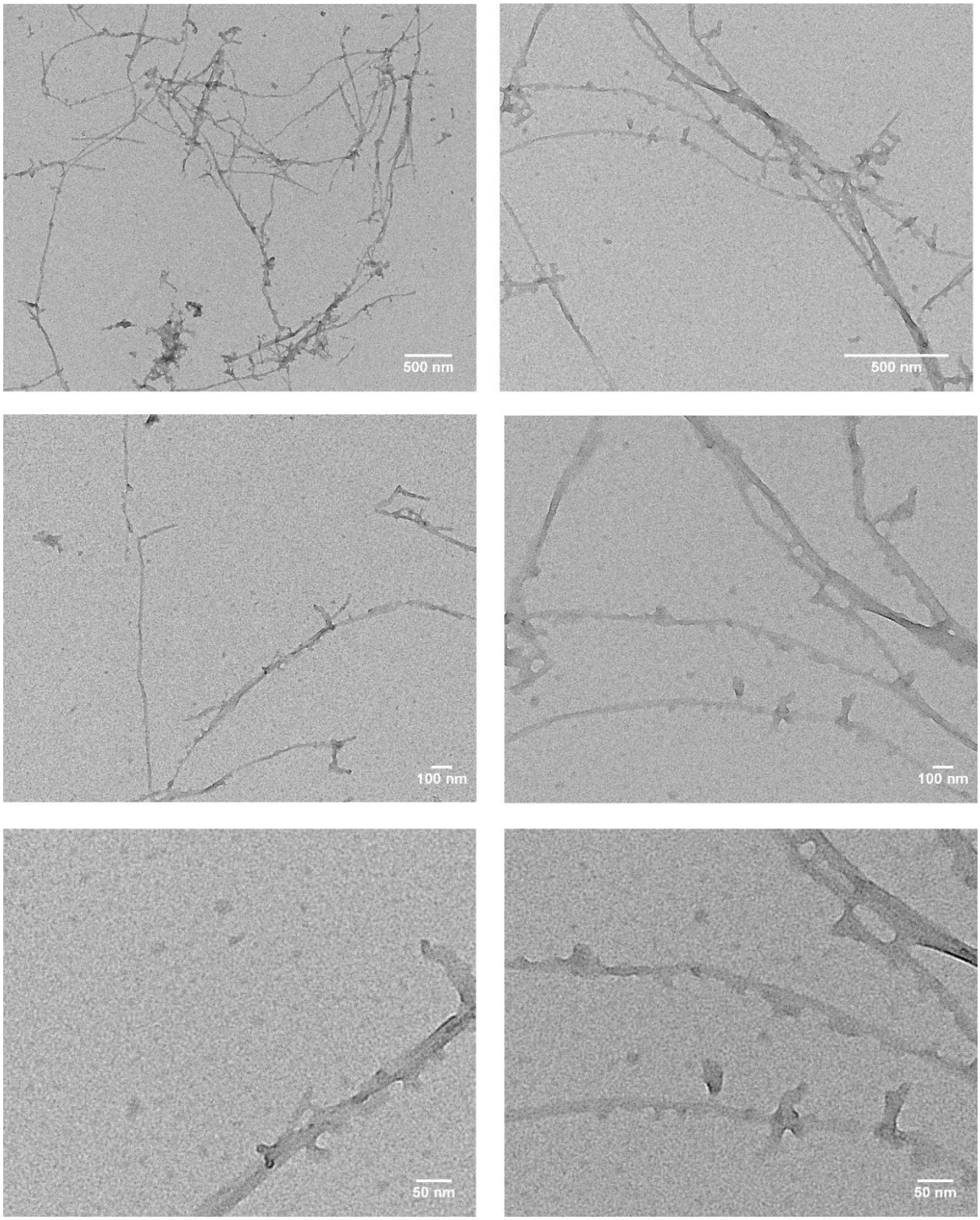

Fig. S10. TEM images of fibril disaggregation. The dual-lalelled 1:1 AF488 and AF59- labelled αS samples are prepared using the same protocol as for the critical aggregation concentration measurements, described in the Supporting Methods section 1.7. After prolonged incubation in fresh buffer solution, both fibrillar and oligomeric aggregates are observed.

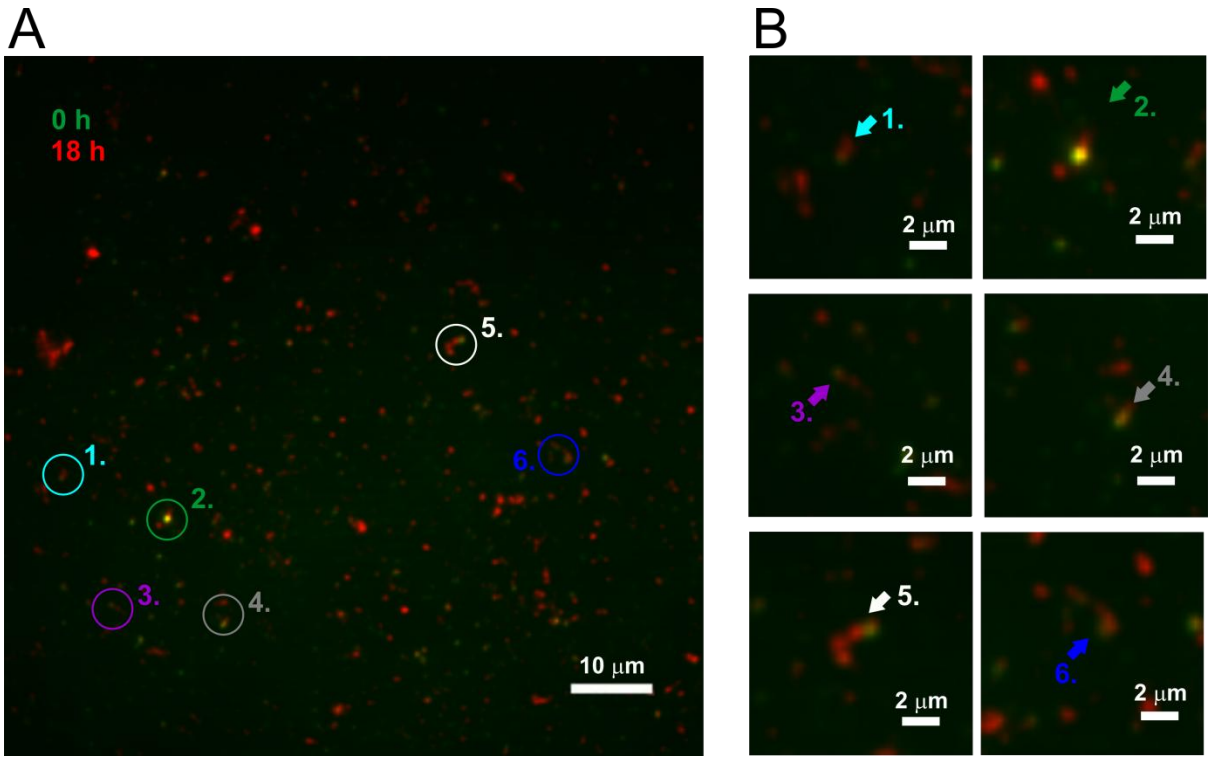

Fig. S11. Representative result of TIRFM on-the-slide seeding experiment (Supporting Methods 1.6.), where high-FRET oligomers are generated and immobilised on poly-lysine surface, and excess of monomeric αS is added. The slide is imaged immediately after monomer addition, 0 hours shown in green, and subsequently the same field of view is re-imaged after 18 hours of static incubation, shown in red. The images at 0 hours and 18 hours are overlapped, and the coincident regions are in yellow. After this time, some of the initially present oligomers elongate to form fibrils, supporting their on-pathway nature. The elongated oligomers are marked by circles in the full field of view in A, and are magnified in B. To note, the experiment is limited by the need to immobilise the oligomers which potentially restricts the accessibility of their sites for the incoming monomer.

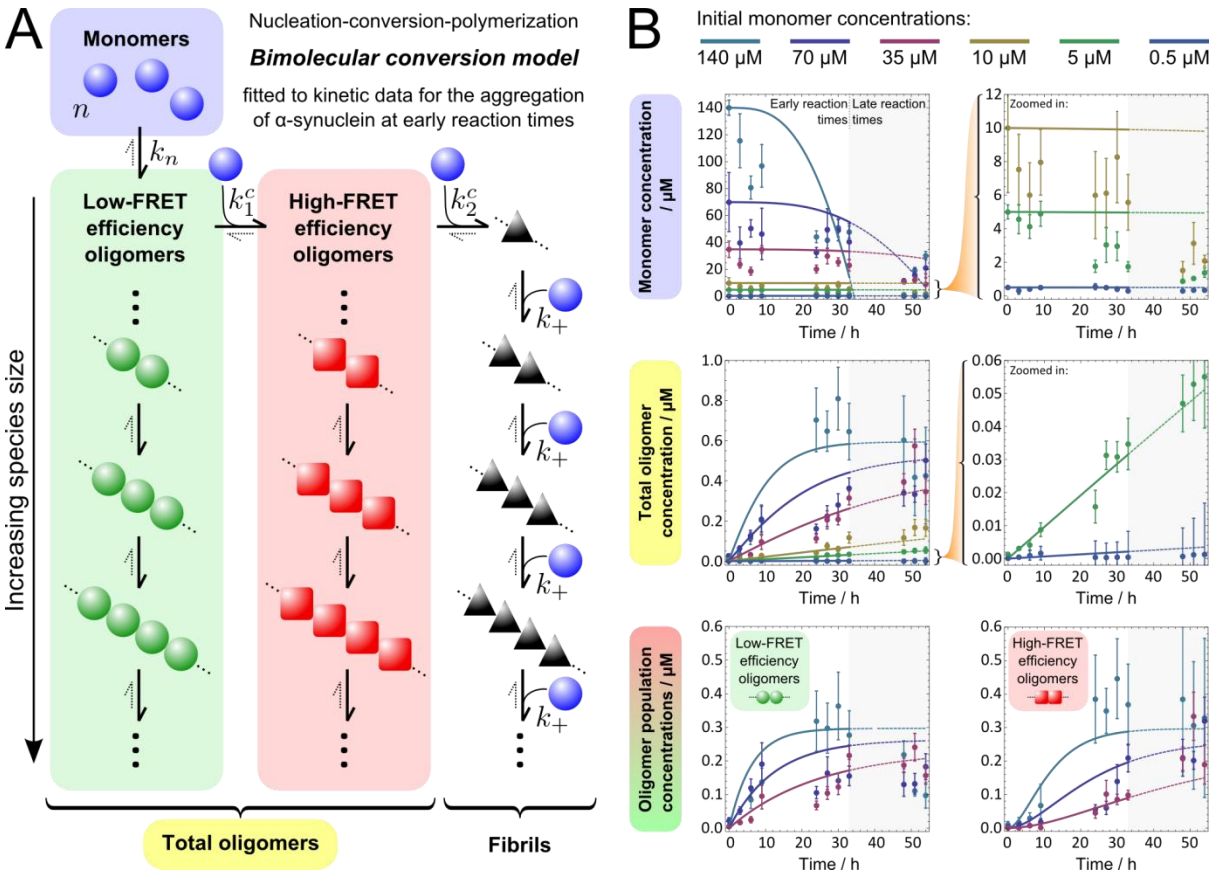

Fig. S12. Modelling the kinetics of αS aggregation. (A) A nucleation-conversion-polymerization model with monomer dependent bimolecular conversions was considered in addition to the unimolecular model presented in Fig. 3. in the Main Text. (B) This model is used to describe the observed populations, whereby monomer units form low-FRET efficiency oligomers with rate constant k_n and an average reaction order of n. These oligomers can then convert to ordered high-FRET efficiency oligomers via a second-order reaction with rate constant k_1^c, with a subsequent final second-order conversion to fibrils with rate constant k_2^c. Fibrils can then recruit single monomer units to grow in a succession of elongation steps, with length-independent rate constant k_+. At early reaction times, reverse reactions and monomer depletion can be neglected, and conversion constants were fixed as equal such that $k_1^c = k_2^c \equiv k_c$. The resulting simplified model, with 4 free parameters, was fitted globally to early-time (up to 33 h) kinetic data showing changes with time in monomeric and oligomeric populations for a range of initial monomer concentrations. The resulting nucleation reaction order is $n = 1.2$, with rate constants $k_n = 1.5 \times 10^{-4}\ \mu\mathrm{M}^{1-n}\mathrm{h}^{-1}$, $k_c = 1.2 \times 10^{-3}\ \mu\mathrm{M}^{-1}\mathrm{h}^{-1}$, and $k_+ = 3.7 \times 10^{-2}\ \mu\mathrm{M}^{-1}\mathrm{h}^{-1}$.

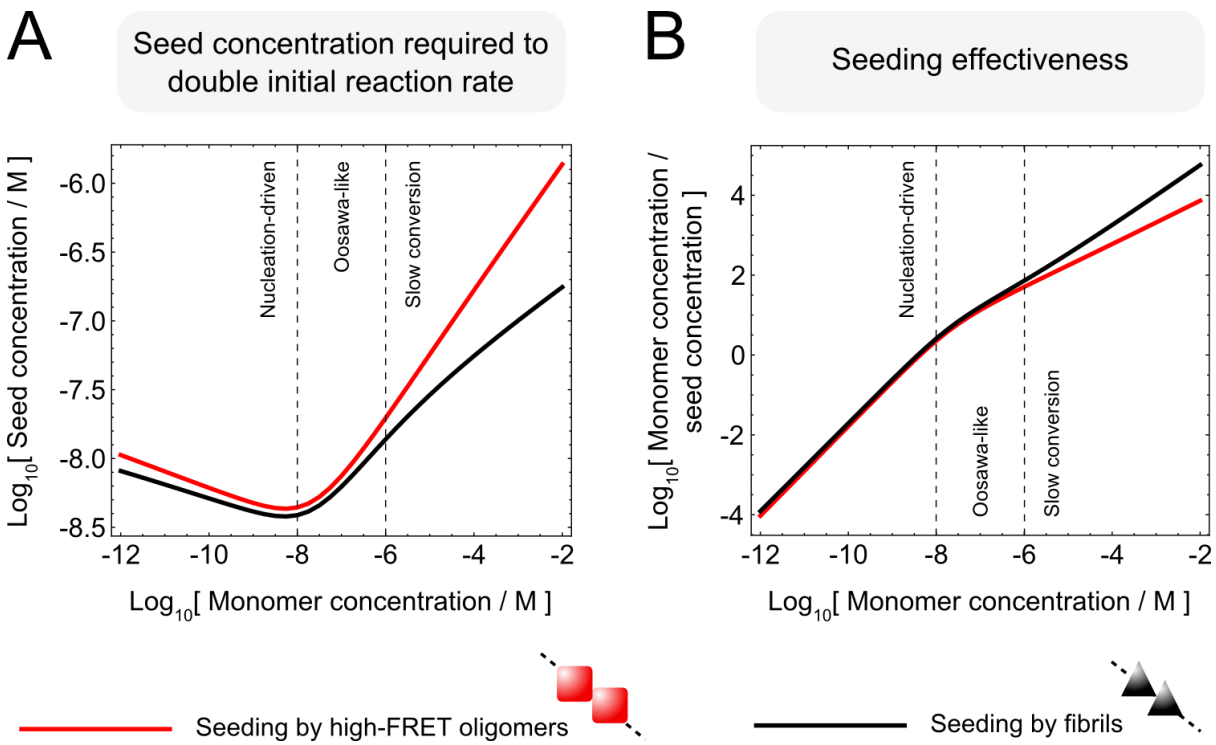

Fig. S13. Simulating seeding scenarios at a range of concentrations. (A) Using our kinetic model with the fitted rate constants (Fig. 3), we are able to evaluate the concentration of seeds required in order to double the initial reaction rate, as measured by production of fibril mass (discussed in the Methods section, Main Text). This calculation was carried out separately for seeding by high-FRET oligomers, and also by small fibrils. (B) "Effectiveness" describes the ratio of the total monomer concentration to seed concentration, providing a measure of how sensitive the system is to seeding. Fibrils are always more effective at seeding than oligomers, as they bypass an extra step in the reaction. Below 10 nM, the reaction kinetics are in the nucleation-driven regime (12) and seeding is relatively ineffective as the reaction bottleneck occurs at fibril elongation. Between 10 nM –1 µM is the Oosawa-like fast conversion regime, where seeding is much more effective due to bypassing the now relatively slow nucleation step, and due to adding extra ends that allow fibril growth. Above 1 µM, seeding is very effective since it bypasses the relatively slow conversion steps. At these concentrations, fibrils become far more effective at seeding, as the extra conversion step they bypass represents a significant bottleneck in the reaction.

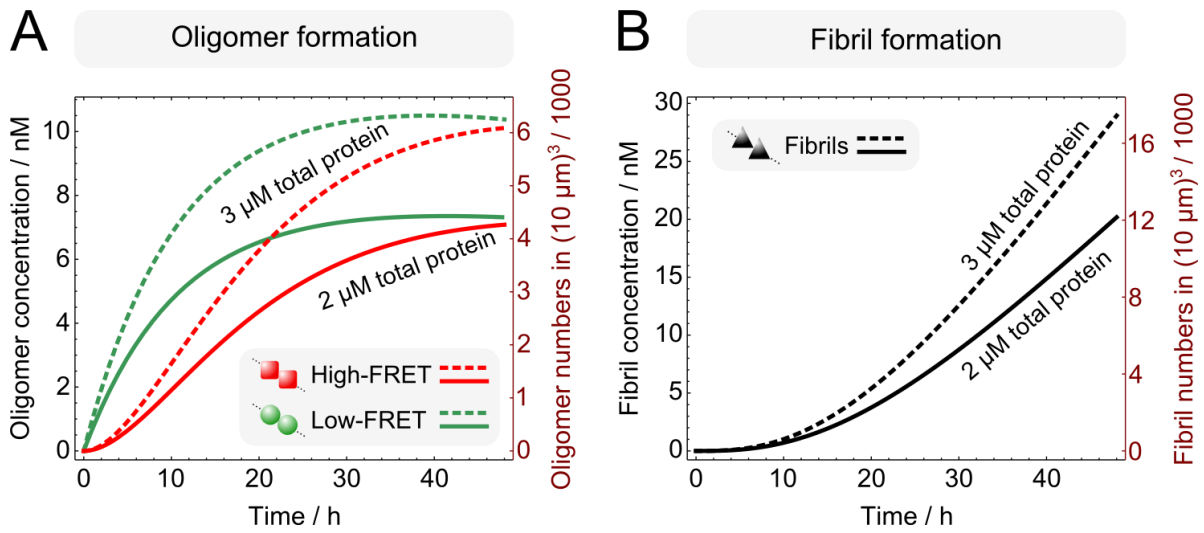

Fig. S14. Predicted production of oligomers (A) and fibrils (B) for 2 µM and 3 µM initial αS concentration over 48 hours. Prediction concentrations are used to calculate numbers of aggregates expected in a volume of $(10\ \mu m)^3$ (scale shown in brown on the right hand side of each plot).

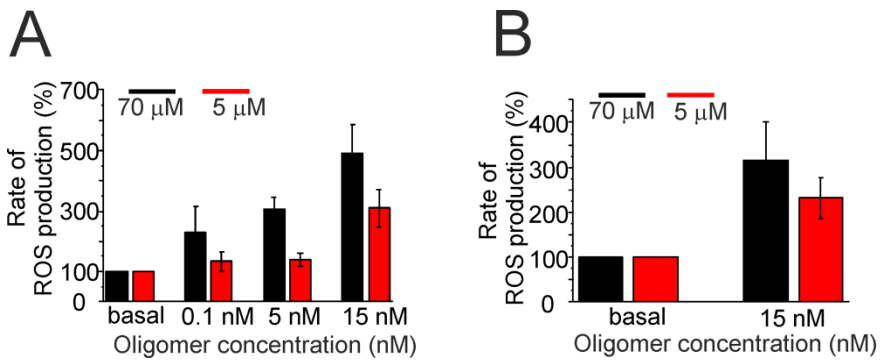

Fig. S15. ROS production in rat primary neuronal cultures, promoted by αS after 29 hours of aggregation. (A) Dose-response assay using Alexa Fluor 647 labelled αs (SD, N=40–60 cells per group). Known values of oligomer concentrations were used to ensure the application of approximately the same concentration of oligomers from either 70 µM sample, or 5 µM sample. Both 70 µM and 5 µM samples produced ROS, shown by an increase in ROS production of 133.4 ± 86.0 % (0.1 nM), 207.0 ± 39.0 % (5 nM) and 392 ± 92.6 % (15 nM) for the 70 µM samples, and 33.4 ± 30.7 % (0.1 nM), 38.4 ± 22.7 % (5 nM) and 207.3 ± 62.6 % (15 nM) increases by 5 µM samples. (B) Measurement (CCD camera) using wt αS, aggregated under identical conditions as the labelled samples. Again, oligomers formed at 70 µM and 5 µM produce ROS, showing 214.6 ± 86.2 % increase by 70 µM samples but only 141.8 ± 46.0 % increase by 5 µM samples (SD, N=40–50 cells per group). Agreement between the experiments using the labelled or unlabelled protein confirms that labelling does not interfere with the ability of αS oligomers to promote ROS production.

3. Supporting References

1. Cremades N*, et al.* (2012) Direct observation of the interconversion of normal and toxic forms of α-synuclein. *Cell* 149(5):1048-1059.
2. Orte A, Clarke R, Balasubramanian S, & Klenerman D (2006) Determination of the fraction and stoichiometry of femtomolar levels of biomolecular complexes in an excess of monomer using single-molecule, two-color coincidence detection. *Anal Chem* 78(22):7707-7715.
3. Yeoman JA, Orte A, Ashbridge B, Klenerman D, & Balasubramanian S (2010) RNA conformation in catalytically active human telomerase. *J Am Chem Soc* 132(9):2852-2853.
4. Horrocks MH*, et al.* (2015) Fast flow microfluidics and single-molecule fluorescence for the rapid characterization of α-Synuclein oligomers. *Anal Chem*. 87(17):8818-26.
5. Shammas SL*, et al.* (2015) A mechanistic model of tau amyloid aggregation based on direct observation of oligomers. *Nat Commun* 6:7025.
6. Jönsson P*, et al.* (2012) Hydrodynamic trapping of molecules in lipid bilayers. *Proc Natl Acad Sci U S A* 109(26):10328-10333.
7. Edelstein A, Amodaj N, Hoover K, Vale R, & Stuurman N (2010) Computer control of microscopes using μManager. *Curr Protoc Mol Biol* Chapter 14:Unit14.20.
8. Narayan P*, et al.* (2013) Single molecule characterization of the interactions between amyloid-β peptides and the membranes of hippocampal cells. *J Am Chem Soc* 135(4):1491-1498.
9. Weimann L*, et al.* (2013) A quantitative comparison of single-dye tracking analysis tools using monte carlo simulations. *Plos One* 8(5):e64287.
10. Chen SW*, et al.* (2015) Structural characterization of toxic oligomers that are kinetically trapped during α-synuclein fibril formation. *Proc Natl Acad Sci U S A* 112(16):E1994-2003.
11. Clarke R, Orte A, & Klenerman D (2007) Optimized threshold selection for single-molecule two-color fluorescence coincidence spectroscopy. *Analytical Chemistry* 79(7):2771-2777.
12. Garcia GA, Cohen SIA, Dobson CM, & Knowles TPJ (2014) Nucleation-conversion-polymerization reactions of biological macromolecules with prenucleation clusters. *Physical Review E* 89(3):6.